Shifting hail hazard under global warming

Timothy H. Raupach[1,2*], Raphael Portmann[3], Christian Siderius[4], Steven C. Sherwood[1,2]

[1]Climate Change Research Centre, UNSW Sydney, Mathews Building Level 4, The University of New South Wales, Sydney, 2051, NSW, Australia.
[2]ARC Centre of Excellence for Climate Extremes, UNSW Sydney, Australia.
[3]Agroscope, Swiss Federal Office for Agriculture, Zurich, Switzerland.
[4]Uncharted Waters Research, Sydney, Australia.

*Corresponding author(s). E-mail(s): timothy.h.raupach@gmail.com;

Abstract

Hailstorms cause significant damage across the globe, but changes to hailstorms in a warming climate are not well quantified. Here, we apply hail proxies to global model projections to quantify changes in the frequency of hail-prone conditions and the effects of those changes on 26 crop types. In projections with 2 °C and 3 °C of mean global warming, hail-prone conditions shift poleward, causing decreases in hail frequency across the mid-latitudes and increases in colder regions. In general, hail-prone frequency decreases in summer and increases in winter, leading to projected increases in the hail-prone proportion of cropping season for winter crops and decreases for summer crops.

Keywords: hail, severe weather, convection, trends, projections

Hailstorms are extreme weather that cause significant damage to assets and crop losses worldwide. Hail and the storms that produce it are expected to be affected by anthropogenic global warming, yet regional studies using observations or projections show geographical inhomogeneities and there remains high uncertainty on the details of any changes [1]. Globally, hail observations are scarce[1], meaning global climatologies generally rely on satellite data [2, 3] or examination of environmental conditions in reanalyses using hail proxies [4]. Here, we global projections of future hail hazard,

using a hail proxies applied to model output from the Coupled Model Intercomparison Project (CMIP6) [5] in a per-degree framework.

Results

Comparison to ERA5 for historical period

Figure 1 shows a comparison between the multi-model, multi-proxy mean of annual hail-prone days for the CMIP6 models, and the multi-proxy mean of annual hail-prone days for the ERA5 reanalyses. Supplementary Figure 2 shows mean annual hail-prone days for the individual models and ERA5 for each proxy. While the CMIP6 models show a wide spread of absolute values, the locations of hail hotspots match well between reanalysis and models. The models MPI-ESM1-2-HR and EC-Earth show similar numbers of hail-prone days to ERA5, while MIROC6, CMCC-CM2-SR5, and CMCC-ESM2 show moderately more and CNRM-CM6-1 and GISS-E2-1-G show significantly more hail activity than ERA5. There are also differences across the selected hail proxies, with the Significant Hail Parameter (SHIP) [6] producing the least hail-prone days and the proxy of Raupach et al. 2023 without extra conditions [7] producing the greatest number of hail-prone days. Given the geographical agreement but differences in absolute numbers of hail-prone days, we consider relative changes per model in the rest of our analyses.

Case study hail-prone day anomalies

Figure 2 shows multi-proxy mean monthly anomalies, derived using ERA5 reanalysis data, in proxy-derived hail-prone days for months with known high occurrences of damaging hailstorms. The proxy produced higher than average numbers of hail-prone days for February 2015 in northern and central India, regions that were affected by hailstorms that caused major losses to wheat crops at this time [8]. Similarly the proxy highlights areas of central and southern Europe as particularly hail-prone in June 2022, when the passage of two low-pressure systems caused hailstorm outbreaks across these regions [9] that broke records for insured losses in France [10]. The proxy also identified April 2015 and October 2022 as unusually hail-prone months in northeast India and western France, respectively (Supplementary Figures 3 and 4); there were reported hailstorms in both regions during the respective months [9, 11]. These case-study results increase our confidence in the ability of the hail proxies, which were trained using data from Australia [7], Italy [12], and the United States [6] **(check)** to identify hail-prone conditions worldwide.

Changes in hail-prone days with warming

Figure 3 shows multi-model, multi-proxy mean changes in annual hail-prone days (differences per model and proxy are shown in Supplementary Figures 5 and 6 for 2 °C and 3 °C warming, respectively). Multi-model, multi-proxy mean changes are shown as relative differences zoomed to selected land areas in Figures 4 and 5. Multi-model, multi-proxy mean differences by season are shown in Supplementary Figure 7.

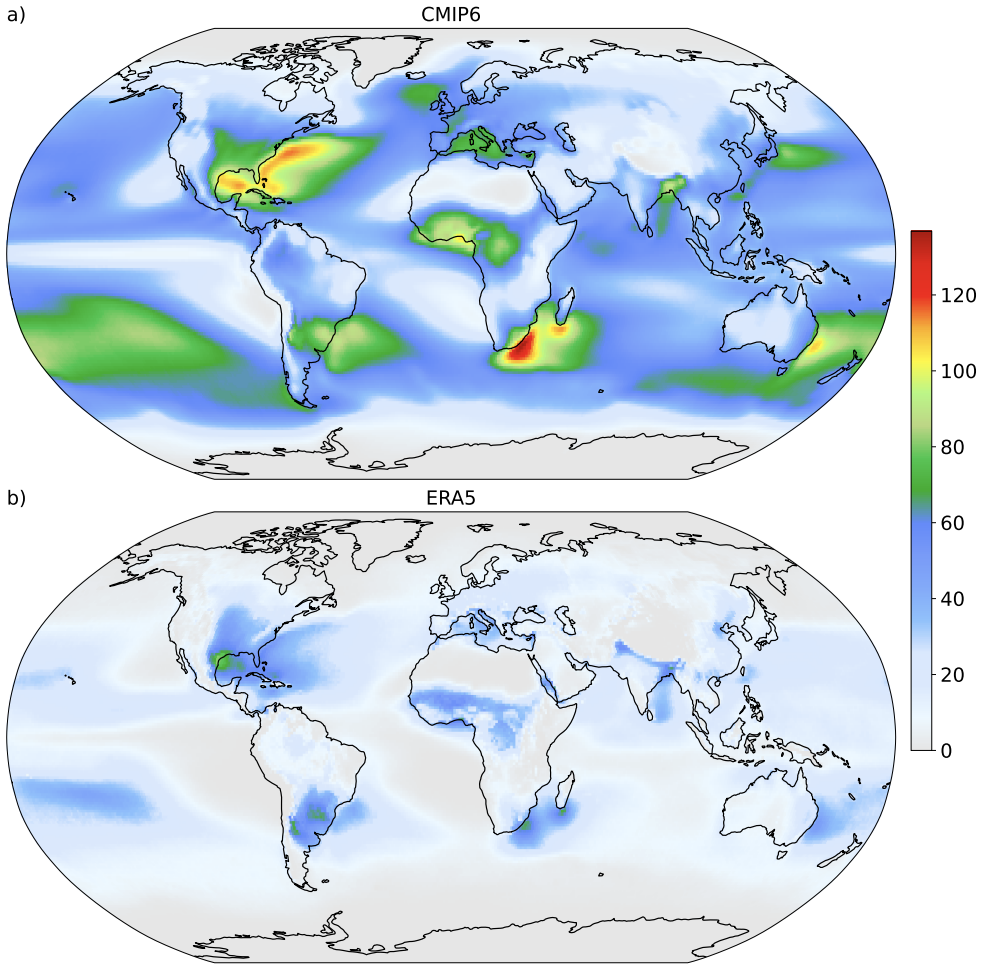

Fig. 1 Hail proxies show known hail-prone regions in both projections and reanalysis. Multi-model, multi-proxy mean annual hail-prone days for CMIP6 models (a), and multi-proxy mean annual hail-prone days for ERA5 reanalysis (b), for four selected proxies over the historical period (1980-1999) at 1 × 1 ° resolution.

Changes in atmospheric ingredients for hail

Supplementary Figures 8 and 9 show changes in hail proxy "ingredients" by epoch.

Changes in hail-prone days in cropping periods

Discussion

Although we show proxy results globally, the proxies used were trained using land-based reports [7, 12] and there is uncertainty in the occurrence of hail in maritime storms [13].

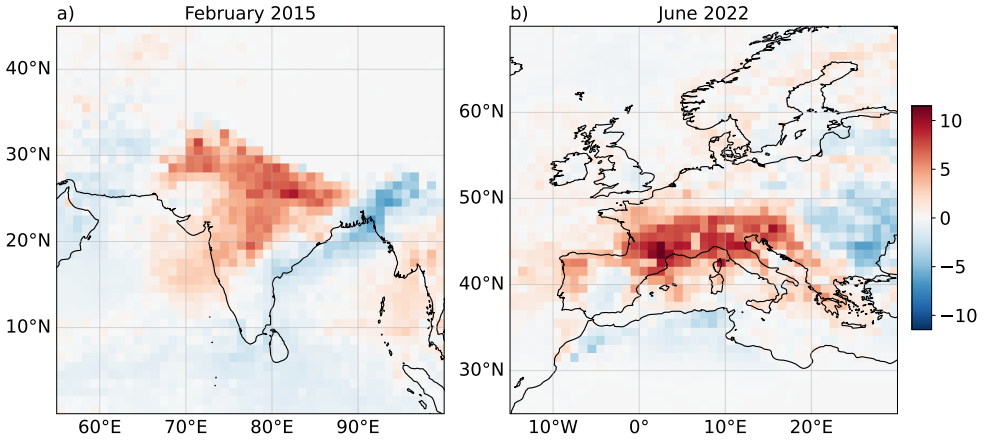

Fig. 2 Hail-proxy anomalies highlight known hail-prone periods. Colours show the monthly anomaly in proxy-derived hail-prone days in ERA5 data with respect to the monthly historical climatology (1980-1999), for the Indian subcontinent in February 2015 (a) and Europe in June 2022 (b). Anomalies for all months in these selected years are shown for the Indian subcontinent and Europe in Supplementary Figures 3 and 4, respectively.

Leung et al., 2023 also observed a northward shift in hailstorms in the US from 2000 (preprint at https://assets.researchsquare.com/files/rs-3217821/v1_covered_a256d1b8-b2e0-41b6-ab9c-e2628059bc91.pdf?c=1699615569.)

Online methods

Data

We used a filtering approach to select models from the Coupled Model Intercomparison Project Phase 6 (CMIP6) [5]. We selected models that contained variables required to calculate convective indices: air temperature at the surface (`tas`) and by model level (`ta`), wind vectors at the surface (`uas` and `vas`) and by level (`ua` and `va`), specific humidity at the surface (`huss`) and by level (`hus`), and surface pressure (`ps`). We filtered for models with a temperal resolution higher than six-hourly (those with "table IDs" of `3hr` or `6hrLev`), and models that were available for both historical and SSP5-8.5 experiments ("experiment IDs" of `historical` or `ssp585`). Further, the models had to be available in the National Computational Infrastructure (NCI) node of the Earth System Grid Federation (ESGF), and had to cover the required epochs. The resulting CMIP6 models, that we used here, are detailed in Supplementary Table 1. If model orography was available in the `orog` variable, it was used; if not, the orography of the historical runs of CNRM-CM6-1 (ensemble r1i1p1f2) was interpolated onto the model grid and used instead [14]. Reanalyses were European Centre for Medium-range Weather Forecasts (ECMWF) reanalysis 5 (ERA5) data [15] on pressure levels [16]. To match the CMIP6 model characteristics, we used global ERA5 data at 00, 06, 12, and 18 UTC for each day from 1980–1999, interpolated to 1×1 ° resolution.

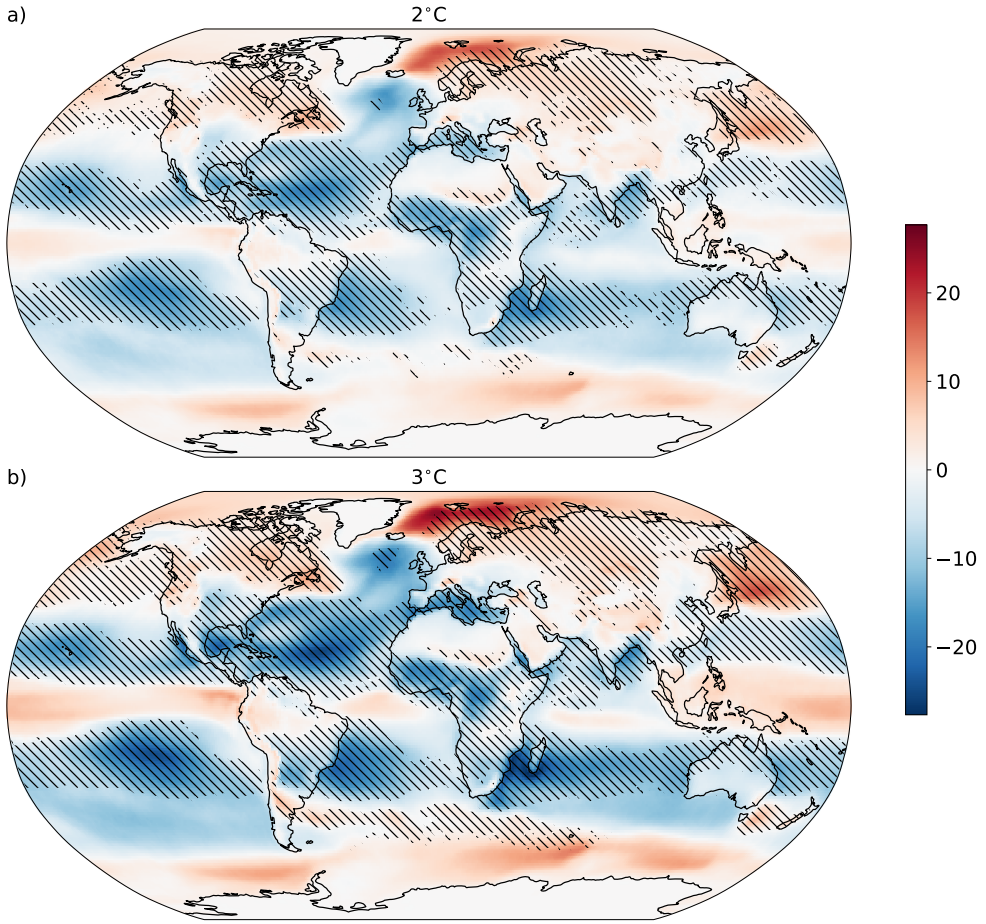

Fig. 3 Hail-prone conditions shift under warming projections. Multi-proxy, multi-model mean changes in annual hail-prone days for 2 °C (a) and 3 °C (b) of global warming. Stippling shows regions in which at least 50% of the model/proxy combinations agreed with the sign of the mean difference and also showed significant differences in the mean ($p < 0.05$ on a t-test on two related samples).

Calculation of convective parameters

Convective parameters were calculated as described for the proxy of Raupach et al., 2023 [7], for each CMIP6 dataset at its native resolution and to ERA5 at the downscaled resolution. For each CMIP6 model, annual and seasonal statistics were calculated, then all statistics were interpolated onto a 1×1 ° spatial grid for comparison.

Application of hail proxies

We applied four hail-specific instability-shear proxies to CMIP6 and ERA5 data. The proxies were those of Raupach et al., 2023 (with and without "extra conditions" to

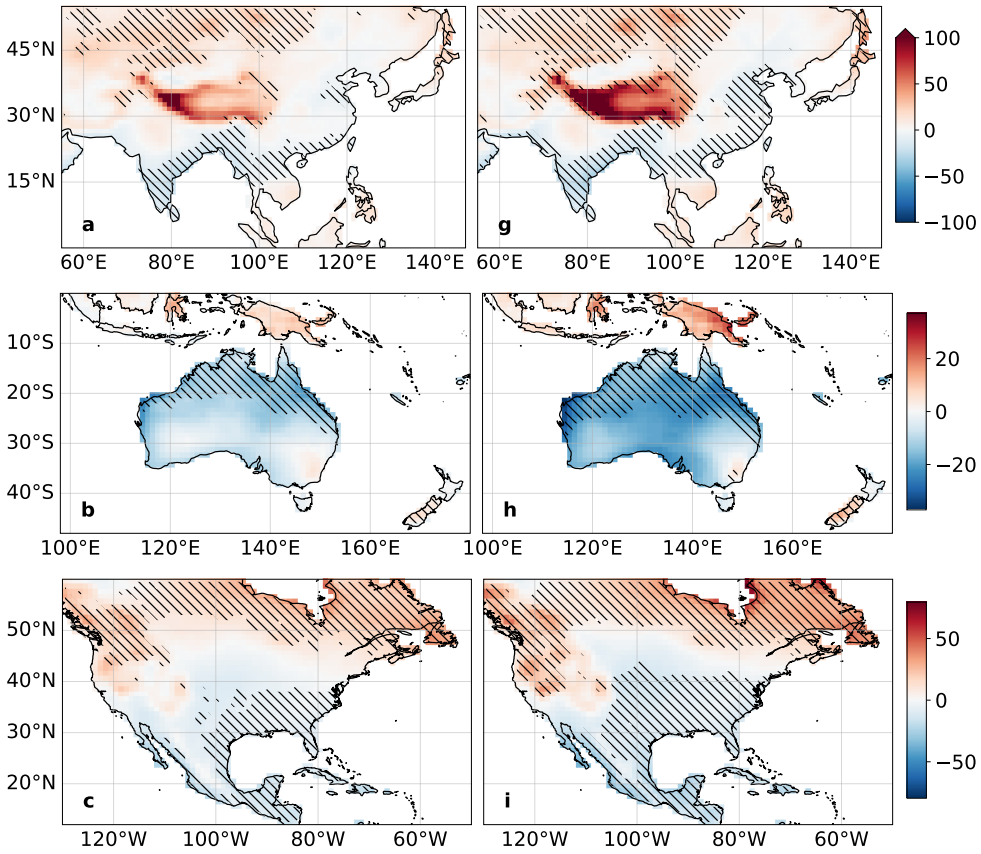

Fig. 4 Multi-proxy, multi-model mean changes in annual hail-prone days by region. Changes are shown as a percentage of historical hail-prone days over land for 2 °C warming (a-c) and 3 °C warming (g-i) for Asia (a, g), Australasia (b, h), and North America (c, i). Stippling as for Figure 3. Colourbars are shared across rows; to increase contrast the colourbar for a and g is truncated.

remove false positives) [7], Eccel et al., 2012 [12], and a threshold of 0.1 on the Significant Hail Parameter (SHIP) [6]. The proxies of Kunz 2007 [17] and Mohr and Kunz, 2013 [18] were tested but were found to produce unrealistically many hail-prone days in tropical regions for which they were not trained [7] (Supplementary Figure 19). Similarly, the threshold of 0.5 on SHIP, as has been used in other studies for severe hail [4], was found to produce too few hail-prone days in comparison with the other proxy results which are for any hail (Supplementary Figure 19), and was therefore excluded here.

Per-degree framework

The historical period used for each model was 1980–1999. The epochs that represented 2 °C and 3 °C warming compared to the historical period were determined per model

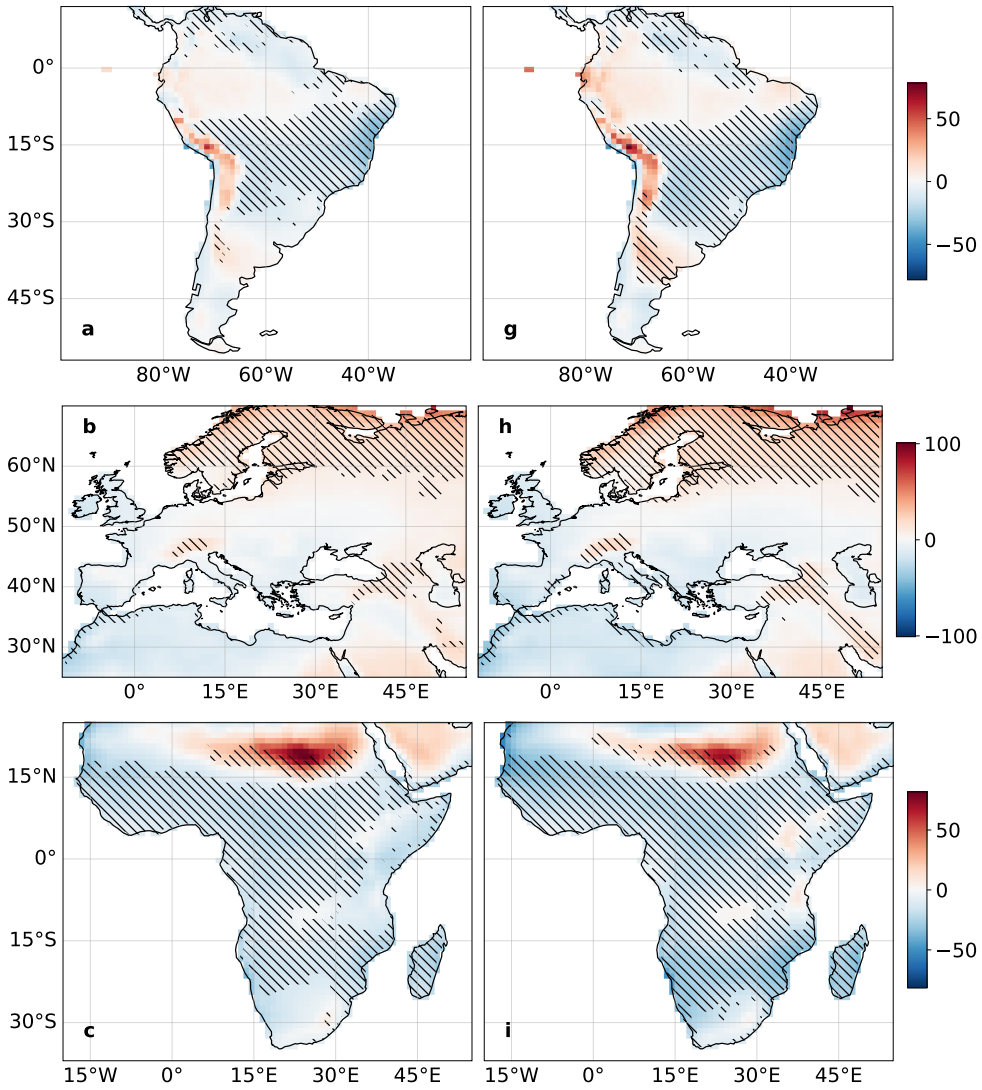

Fig. 5 As for Figure 4 but for South America (a, g), Europe (b, h), and Africa (f, i).

using 20-year running means of monthly global average temperature anomalies. The date ranges for each epoch are shown in Supplementary Figure 20.

Data availability. MIRCA2000 data are available with identifier https://doi.org/10.5281/zenodo.7422506.

Code availability. Convective indices were calculated using `xarray_parcel` by T. H. Raupach (https://doi.org/10.5281/zenodo.8088497) **(Update version with new xarray release)**. Warming levels were calculated using code by T. H. Raupach **(ref)**.

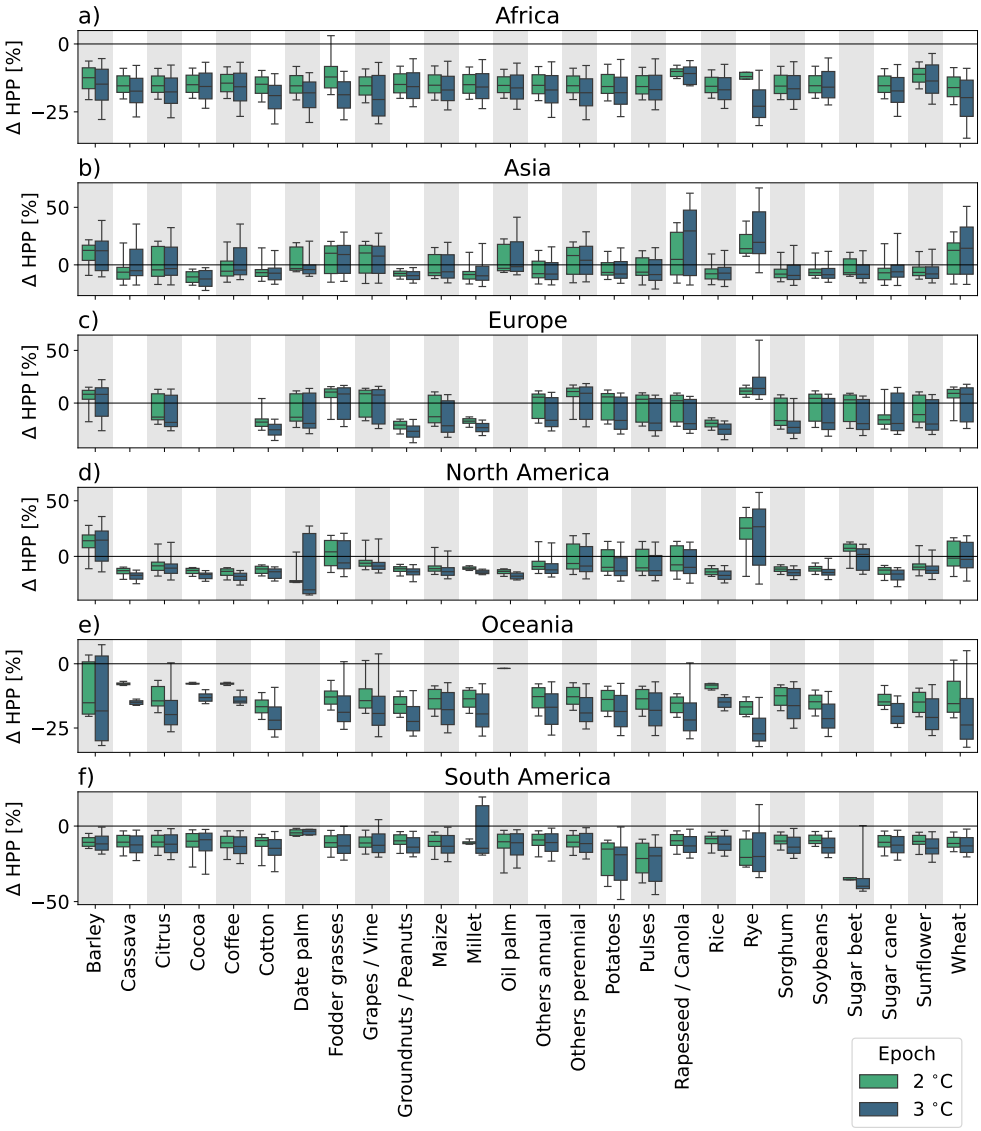

Fig. 6 Distributions of significant changes in hail-prone crop proportion by crop, epoch, and world region. Regions are defined as in Figure 4. Changes multi-model, multi-proxy mean changes shown as a percentage of the multi-model, multi-proxy mean historical hail-prone crop proportion. Significant changes are those for which at least 50% of the model/proxy combinations agreed with the sign of the mean difference and also showed significant differences in the mean ($p < 0.05$ using Welch's t-test). Coloured boxes show inter-quartile ranges, whiskers show 10th-90th percentile ranges.

Acknowledgments. This research was undertaken with the assistance of resources and services from the NCI, which is supported by the Australian Government.

Competing interests. The authors declare no competing financial or non-financial interests.

Author contributions.

References

[1] Raupach, T. H. *et al.* The effects of climate change on hailstorms. *Nat. Rev. Earth Environ.* **2**, 213–226 (2021).

[2] Cecil, D. J. & Blankenship, C. B. Toward a global climatology of severe hailstorms as estimated by satellite passive microwave imagers. *J. Climate* **25**, 687–703 (2012).

[3] Bang, S. D. & Cecil, D. J. Constructing a multifrequency passive microwave hail retrieval and climatology in the GPM domain. *J. Appl. Meteorol.* **58**, 1889–1904 (2019).

[4] Prein, A. F. & Holland, G. J. Global estimates of damaging hail hazard. *Weather Clim. Extremes* **22**, 10–23 (2018).

[5] Eyring, V. *et al.* Overview of the Coupled Model Intercomparison Project Phase 6 (CMIP6) experimental design and organization. *Geosci. Model Dev.* **9**, 1937–1958 (2016).

[6] NOAA SPC. Significant hail parameter. https://www.spc.noaa.gov/exper/mesoanalysis/help/help_sigh.html (2022). National Oceanographic and Atmospheric Administration National Weather Service Storm Prediction Center, accessed 21 June 2022.

[7] Raupach, T. H., Soderholm, J., Protat, A. & Sherwood, S. C. An improved instability–shear hail proxy for australia. *Mon. Weather Rev.* **151**, 545–567 (2023).

[8] Singh, S. K., Saxena, R., Porwal, A., Ray, N. & Ray, S. S. Assessment of hailstorm damage in wheat crop using remote sensing. *Curr Sci India* **112**, 2095–2100 (2017).

[9] Pucik, T. Major hailstorms of 2022 (2023). URL https://www.essl.org/cms/major-hailstorms-of-2022/. Accessed 2024-01-10.

[10] Soyka, T. Severe 2022 hail damage in france sets new benchmarks, underscores shift of risk and calls for pricing adjustments (2023). URL https://www.swissre.com/risk-knowledge/mitigating-climate-risk/hail-damage-risk-france-2022.html. Accessed 2024-01-10.

[11] Chattopadhyay, N., Devi, S. S., John, G. & Choudhari, V. Occurrence of hail storms and strategies to minimize its effect on crops. *Mausam* **68**, 75–92 (2017).

[12] Eccel, E., Cau, P., Riemann-Campe, K. & Biasioli, F. Quantitative hail monitoring in an alpine area: 35-year climatology and links with atmospheric variables. *Int. J. Climatol.* **3**, 503–517 (2012).

[13] Knight, C. A. & Knight, N. C. in *Hailstorms* (ed.Doswell, C. A.) *Severe Convective Storms* 223–254 (American Meteorological Society, Boston, MA, 2001).

[14] Bracegirdle, T. J. *et al.* Twenty first century changes in Antarctic and Southern Ocean surface climate in CMIP6. *Atmos. Sci. Lett.* **21**, e984 (2020).

[15] Hersbach, H. *et al.* The ERA5 global reanalysis. *Q. J. Roy. Meteor. Soc.* **146**, 1999–2049 (2020).

[16] Hersbach, H. *et al.* ERA5 hourly data on pressure levels from 1979 to present (2018). Copernicus Climate Change Service (C3S) Climate Data Store (CDS).

[17] Kunz, M. The skill of convective parameters and indices to predict isolated and severe thunderstorms. *Nat. Hazards Earth Sys.* **7**, 327–342 (2007).

[18] Mohr, S. & Kunz, M. Recent trends and variabilities of convective parameters relevant for hail events in Germany and Europe. *Atmos. Res.* **123**, 211–228 (2013).